Published in final edited form as:
Neurobiol Aging. 2013 May ; 34(5): 1343–1354. doi:10.1016/j.neurobiolaging.2012.10.024.

Cascade of tau toxicity in inducible hippocampal brain slices and prevention by aggregation inhibitors

Lars Messing[1], **Jochen Martin Decker**[#1], **Maria Joseph**[#1], **Eckhard Mandelkow**[1,2,3], and **Eva-Maria Mandelkow**[1,2,3,*]

[1]German Center for Neurodegenerative Diseases (DZNE), Ludwig-Erhard-Allee 2, 53175 Bonn, Germany

[2]CAESAR Research Center, Ludwig-Erhard-Allee 2, 53175 Bonn, Germany

[3]Max-Planck-Institute for Neurological Research (Cologne), Hamburg Outstation, c/o DESY, Notkestrasse 85, 22607 Hamburg

[#] These authors contributed equally to this work.

Abstract

Mislocalization and aggregation of the axonal protein Tau are hallmarks of Alzheimer disease and other tauopathies. Here, we studied the relationship between Tau aggregation, loss of spines and neurons, and reversibility by aggregation inhibitors. To this end we established an in vitro model of tauopathy based on regulatable transgenic hippocampal organotypic slice cultures prepared from mice expressing pro-aggregant $Tau_{RD}\Delta K$. Transgene expression was monitored by a bioluminescence reporter assay. Abnormal Tau phosphorylation, mislocalization of exogenous and endogenous Tau into the somatodendritic compartment, followed by reduction of dendritic spines, altered morphology from mushroom-shaped to thin spines, dysregulation of Ca^{++} dynamics, Tau aggregation, neuronal loss and elevated activation of microglia. Neurotoxicity was mediated by Caspase-3 activation and correlated with the expression level of pro-aggregant $Tau_{RD}\Delta K$. Finally, Tau aggregates appeared in areas CA1 and CA3 after three weeks in vitro. Neurodegeneration was relieved by aggregation inhibitors or by switching off transgene expression. Thus the slice culture model is suitable for monitoring the development of tauopathy and the therapeutic benefit of anti-aggregation drugs.

Keywords

Aggregation; Aggregation-inhibitory drugs; Hippocampus; Organotypic slice culture; Tau pathology

[*]**Corresponding Author**: eva.mandelkow@dzne.de.

Disclosure statement
The authors have nothing to disclose.

Europe PMC Funders Author Manuscripts

1 Introduction

Tau, a microtubule-associated protein in the brain, aggregates abnormally in Alzheimer disease (AD) and other neurodegenerative tauopathies (Ballatore et al, 2007; Morris et al, 2011). Tau is highly soluble and adopts a natively unfolded structure in solution. In Tau fibers of AD (termed paired helical filaments, PHFs), short motifs of Tau adopt a ß-conformation which leads to interactions with other Tau molecules (von Bergen et al., 2000). The spreading of Tau aggregates correlates well with cognitive decline in AD (Braak & Braak, 1994). Abnormal phosphorylation and mislocalization of Tau is an early hallmark of neurodegeneration and precedes aggregation (Braak & Braak, 1994; Giannakopoulos et al, 2003; Gomez-Isla et al, 1997). Mutations within the Tau repeat domain, like the FTDP-17 mutation ΔK280 (Rizzu et al, 1999) increase Tau's propensity for β-structure and promote aggregation in vitro (Barghorn et al, 2000). Mechanisms of Tau-mediated cell death are still under debate (Spires-Jones et al, 2011). Caspase activation and caspase-cleaved Tau was found in tauopathy models (Rohn et al, 2002; Gamblin et al, 2003) suggesting that apoptosis plays a role in Tau-induced cell death. Others found early caspase activation, following Tau cleavage thereby initiating tangle formation. After a new tangle has formed, the neuron remained alive and caspase activity seemed to be suppressed (de Calignon et al, 2010). A loss or alteration of dendritic spines has been described in patients with neurodegenerative disorders and is thought to be responsible for cognitive deficits but the underlying mechanisms are poorly understood. To clarify some of these issues we used transgenic hippocampal organotypic slices from pro-aggregant Tau_{RD}ΔK280 mice to study the relationship between Tau expression, physiological dysfunction, aggregation and finally neurotoxicity and their prevention by Tau aggregation inhibitors. The hippocampus is highly affected in AD (Braak & Braak, 1991; Smith et al, 2009). Furthermore, the remarkable ability for regeneration makes hippocampal organotypic slices suitable for long term cultivation (Gahwiler, 1988; Stoppini et al, 1991). Such slices from young animals share many similarities with acute slices, e.g. development of dendritic spines (De Simoni et al, 2003), but can be kept for weeks and allow extended monitoring and experimental manipulation without the complications of the blood-brain barrier. These preparations are therefore particularly suitable to analyze the time course of pathological events and allow testing of potential drugs. In the present study we show that Tau can aggregate in hippocampal slice cultures, that Tau aggregation and toxicity occurs in parallel, and that aggregation inhibitors can abolish both aggregation and toxicity. Moreover, alterations and loss of dendritic spines occurred before aggregation and cell death. Our findings suggest that Tau pathology starts with missorting of Tau into the somatodendritic compartment, resulting in reduction and changes in morphology of dendritic spines. At the same time we observed a reduction of Ca++ influx evoked by membrane depolarization in Tau_{RD}ΔK slices. At later stages Tau aggregates and cell death accompanied by caspase-3 activation were observed. Compound bb14, a Tau aggregation inhibitor from the rhodanine class, was able to prevent the development of Tau pathology, i.e. phosphorylation, missorting, aggregation, spine loss; it preserved Ca++ dynamics and protected neurons against toxicity and cell death.

2 Materials and Methods

Transgenic mice expressing the human Tau four-repeat domain with the FDTP-17 mutation ΔK280 (Tau_{RD}ΔK, 129 residues, M-Q244-E372 without K280) and reporter gene firefly luciferase under control of a Tet-operon response element (tetO) (Mocanu et al, 2008), were crossed with CaMKIIα-tTA mice (Mayford et al, 1996) to generate a regulatable Tet-off system. For histochemical and behavioral details on these double transgenic mice see Sydow et al, 2011. Animals were housed and tested according to standards of the German Animal Welfare Act.

Hippocampal organotypic slice cultures were prepared following Stoppini et al (1991), with modifications. Briefly, 7-10 days old mice were decapitated, brains were rapidly removed and hippocampi dissected at 4°C. A McIIwain tissue chopper (Gabler, Bad Schwabach; Germany) was used to prepare 400 μm thick transverse slices which were transferred to semi-porous cell culture inserts (Millipore, Bedford, MA, 0.4 μm). Inserts containing 6-8 slices were placed in six well culture trays containing 1 ml of culture media (50% MEM, 25% HBSS, penicillin/streptomycin (all from PAA, Austria), 25% horse serum, 4.5 mg/ml glucose (Sigma, Germany), pH 7.4). The culture medium was changed on the first day after preparation and afterwards every 3rd day. Slices were kept in culture for 3 - 4 weeks. Suppression of the human Tau transgene was achieved by adding doxycycline hydrochloride (Sigma, Germany) to the culture media (final concentration 2 μg/ml). The treatment with doxycycline was carried out from DIV1 unless stated otherwise. During treatment, doxycycline was refreshed every 3rd day, simultaneously with full medium change.

Immunohistochemistry

Slice cultures were left attached on the Millicell membrane and stained as free-floating sections in 6-well plates. Cultures were first fixed with 4% paraformaldehyde in PBS (PAA, Austria) for 2 h at 4°C. After washing with cold PBS, slices were permeabilized by 0.4% TritonX-100/PBS for 90 min at RT. Slices were then blocked with 5% BSA for 2 h and afterwards incubated with primary antibody diluted in PBS for 2-3 days at 4°C. After washing with PBS, slices were incubated with secondary antibody for 2 d at 4°C. After washing, slices were mounted with Permafluor mounting solution (Beckman Coulter, Paris, France), cover-slipped and dried before imaging. The following primary antibodies were used: monoclonal anti-neuronal nuclei (NeuN) antibody (Chemicon International, Temecula, CA) (1:500), pan-Tau antibody K9JA (Dako, Hamburg, Germany, Nr. A0024 (1:1000)), MAP2a/b (AP20, Sigma-Aldrich, Germany (1:200)),12E8 (1:1000) for phosphorylated S262/S356 Tau (gift from Dr. P. Seubert, Elan Pharma, South San Francisco, CA); PHF1 antibody for phosphorylated S396/404 Tau (gift from Dr. Peter Davies, Albert Einstein College, NY) and anti-Iba1 (Wako Chemicals, Germany) (1:1000). All fluorescent (goat anti-rabbit/mouse cyanine 2, 3 and 5)-labeled secondary antibodies were from Dianova (Hamburg, Germany) (1:1000). Thioflavine-S (ThS) (Sigma, Germany) staining was done as previously described (Mocanu et al, 2008). Briefly, fixed slices were incubated in 0.05% ThS for 8 min, washed twice with 80% ethanol, followed by 3 washing steps with ddH_2O.

Diolistic labeling for spine detection

The lipophilic tracer 1,1'-dioctadecyl-3,3,3',3'-tetramethylindocarbocyanine perchlorate (Dil, Invitrogen, Germany) was used to investigate dendritic spines in Tau transgenic or control slice cultures (Moolman et al, 2004). Gold particles (1.6 μm radius) were coated with Dil by sonication for 20 min at RT. Dil coated gold particles were applied under high pressure (650 psi) in living slice cultures by using a helium pump (BioRad, Germany). Cultures were immediately fixed in fixation solution and stored at 4°C for at least 48 h before imaging by using TRITC-filter settings. The spine density of apical dendrites of CA1 pyramidal neurons was estimated after 10 and 20 days *in vitro.* Apical dendritic branches (>150 μm from cell soma) were imaged by high resolution confocal microscopy (see below). Spine density was determined from Z-stacks using ImageJ (NIH). Spines were further classified by the 3D image analysis software NeuronStudio (Rodriguez et al, 2008) which allows reconstruction of neuronal structures from confocal images and yields classification of spines into thin, stubby and mushroom.

Microscopy

Images were acquired with an Olympus laser scanning microscope FV1000 (Olympus, Tokyo), equipped with confocal laser scanning unit, argon (Ar; 488 nm) and helium/neon (He/Ne 543 nm and 633 nm). For 2 or 3 channel imaging, images were acquired via sequential scanning. Image stacks were collected for the whole hippocampus at lower magnification and for all hippocampal subfields at higher magnifications. Digital zoom was used for fluorescent dye tracing of single neurons and spines. Maximum projection images were generated from resulting *Z* stacks using ImageJ software (NIH).

Ca^{++} imaging experiments

For Ca++ imaging experiments, organotypic slices were used at DIV15. Slices were loaded with Fura-2AM (Invitrogen, Carlsbad, US) at a concentration of 100 μM at 37°C for 30 min. Fura-2 AM stock solution (5 mM dissolved in DMSO) was added to the culture dish containing 1 ml of medium. After loading, slices were washed with HEPES-buffered saline (HBSS; 130mM NaCl, 5.4mM KCl; 10mM HEPES, 25mM glucose, 1.8mM $CaCl_2$, 1mM $MgCl_2$; ph 7.4) for another 30 min to allow complete de-esterification of the Fura dye. After washing, cultures were transferred to a submerged imaging chamber of an Examiner. A1 microscope (Zeiss, Germany). Fura-2 fluorescence was imaged at RT in HBSS, using a 10x water-immersion objective. Prior to the experiments the level of auto fluorescence of the slices was addressed, by imaging cultures in the absence of Fura-2 AM. Resulting fluorescence units (FU) were ~300% lower than in the presence of Fura-2 AM. The emission of Fura-2-loaded pyramidal neurons in area CA3 was collected at 510 nm after excitation at 340 and 380 nm respectively with a Sutter DCIV shutter (Sutter Instrument Co., Navato, CA, USA). Images were taken at a rate of 1 Hz. For baseline intracellular Ca++ levels we recorded a 30 s period following a perfusion with high potassium (HBSS containing 180 mM KCL) for additional 30 s. As a KCl stimulation control we stimulated slices with HBSS alone and did not observe any changes in Ca++ concentrations. Also the restitution of basal Ca++ levels after washing out the KCl stimulation was tested. Analysis was performed offline, using 10 regions of interests (ROIs) with constant diameter inside a)

stratum radiatum b) pyramidal cell layer and c) stratum oriens. For each slice we performed an internal background substraction and averaged the ROI values of the different hippocampal layers and normalized with their individual baseline. Absolute intracellular Ca ++ concentrations were calculated from the ratio of emitted fluorescence (510 nm) after excitation at 340 nm and 380 nm in HBSS, by calibrating with the standard Grynkiewicz formulary (Grynkiewicz et al., 1985). The *Kd* value was calculated by using Invitrogen Fura-2 calibration Kit.

Biochemistry of slice cultures

To estimate protein expression, cultured hippocampal slices (6–8, prepared and pooled from the same animal) were homogenized in lysis buffer [50 mM Tris-HCl, pH 7.4, 10% glycerol, 1% NP-40, 5 mM DTT, 1 mM EGTA, 20 mM NaF, 1 mM Na_3VO_4, 150 mM NaCl, protease inhibitors (Complete Mini; Roche, Indianapolis, IN), 5 mM CHAPS (3-[(3-cholamidopropyl)dimethylammonio]-1-propanesulfonate), 100 U/ml benzonase, 5 μm okadaic acid]. Slice homogenates were resolved by SDS-PAGE (17% polyacrylamide gels) and transferred to polyvinylidene fluoride (PVDF) membranes (Millipore, Bedford, MA). The membrane was incubated in 5% non-fat milk in TBS-Tween for 1 h at RT, washed with TBS-Tween the next day and incubated overnight in primary antibody solution at 4°C. The membrane was washed with TBS-Tween and incubated with the secondary antibody (Dako, Germany) coupled to horseradish peroxidase (HRP) for 1 h at RT. The membrane was developed by ECL Western Blotting Detection Kit (GE Healthcare, USA) and analyzed by densitometry (LAS 3000; AIDA software; Raytest, Straubenhardt, Germany). The following antibodies were used: monoclonal anti-neuron-specific beta-III tubulin antibody (R&D Systems, Minneapolis, MN) (1:1000); pan Tau antibody (DakoCytomation, Carpinteria, CA) (1:5000); 12E8 (1:2500) for phosphorylated S262/S356 Tau (gift from Dr. P. Seubert, Elan Pharma, South San Francisco, CA), anti-ß actin (Sigma, Germany) (1:10.000) and secondary antibodies, HRP-anti-rabbit and HRP-anti-mouse (DakoCytomation, Carpinteria, CA).

Extraction of sarkosyl-insoluble Tau from cultured slices was done as described (Mocanu et al, 2008). Cultured slices at DIV25 were homogenized in 10-30μl of cold buffer H and centrifuged at 27,200x*g* for 20 min at 4°C. The pellet was again homogenized in the same volume of buffer H and centrifuged a second time using the same settings. Both supernatants were combined, adjusted to 1% (w/v) *N*-lauroylsarcosine, and incubated at 37°C with shaking for 2 h. After centrifugation at 150,000x*g* for 35 min at 20°C, the supernatant was collected and the pellet resuspended in 10-15μl 50mM Tris-HCl, pH7.4. Supernatant and pellet fractions were analyzed by densitometry (LAS 3000; AIDA software; Raytest) after western blotting with pan-Tau antibodies (Dako, Germany).

Cytotoxicity was assessed by the LDH assay using the Roche Cytotoxicity Detection Kit (Roche Diagnostics, Mannheim, Germany). Slice culture media (serum free) were collected and treated as prescribed. Absorbance at 492 nm (indicating dying cells) was assayed in 96-well plates (plate reader Tecan Safire, Switzerland). For further investigation of neurotoxicity, slice cultures were stained against NeuN to visualize neurons in the DG and CA regions. NeuN positive cells were blindly counted within the granule and pyramidal cell layer of area CA1, CA3 and DG using ImageJ (NIH). Caspase-3 activity was determined

fluorimetrically by the EnzChek Caspase-3 Assay Kit with Z-DEVD-AMC substrate (Molecular Probes). Pooled slice cultures (6 slices/sample) were homogenized and treated as prescribed. The assay was performed in 96-well microplates and read on a fluorescence plate reader (Tecan Safire) at excitation 342 nm and emission 441 nm. Caspase-3 activity was normalized relative to total protein. As a positive control, slices were treated with 0.5 μM staurosporine, an inducer of apoptosis (Calbiochem, USA), 24 hours prior to measurement.

Assessment of luciferase activity

Since the mouse line was generated using a bidirectional promoter to express both $Tau_{RD}\Delta K$ and the reporter protein Firefly luciferase, its enzymatic activity can be used to quantify the expression levels and regional distribution (Contag, 2007). Photon emission was detected with a luminometer (IVIS Spectrum) at 560-660 nm (Caliper Life Sciences, Germany) after incubation of cultures with 470 μM of the luciferase substrate D-luciferin (Caliper Life Sciences, Germany) and measured after 10, 15, 20, 25 and 30 days in culture. The chemiluminescent reagent XenoLight RediJect Inflammation probe (Caliper Life Sciences, Germany) was used to track the inflammation status by incubation of slices with 400 μM of reagent and measuring photon emission 5 min later by a luminometer.

Drug application

Slice cultures were treated with compound bb14, a rhodanine-based Tau aggregation inhibitor identified in previous screens (Pickhardt et al, 2005; Bulic et al, 2007). Compound bb14 was dissolved in 100% DMSO and added to the culture media at a final concentration of 15 μM (0.15% (v/v) DMSO). Untreated control groups received the same amount of DMSO alone. In all experiments treatment was done for the entire cultivation period starting at DIV1. During treatment, the compound was refreshed one day after preparation and afterwards every 3rd day, simultaneously with full medium change. The L-VGCC inhibitor nifedipine and NMDAR blocker APV (both from Tocris Biosciences, USA) were dissolved in DMSO and diluted in HBSS. Slices were treated either with 100 μM APV or 20 μM nifedine 15 min before and during the Ca^{++} imaging experiments. The caspase 3/7 inhibitor DEVD-CHO (Molecular Probes, USA) was applied at 30 μM from DIV10 - DIV20 and refreshed every 3rd day.

Statistical analysis

Statistical analysis was done by using the statistics software Prism5 (GraphPad, La Jolla, CA, USA). Evaluation of data was performed either by *Student's t-test* or One way ANOVA followed by *Tukey's post-hoc* test as indicated. Data are shown as mean ± SEM. p values are as follows: *$p < 0.05$, **< 0.01, and ***$p < 0.001$.

3 Results

3.1 Distribution of pro-aggregant $Tau_{RD}\Delta K$ in organotypic slice cultures

$Tau_{RD}\Delta K$ has a high propensity for β-structure and strongly promotes Tau aggregation in vitro and in a cell model (Barghorn et al, 2000; Khlistunova et al, 2006; (Fig. 1A)). Western blot analysis with the pan-Tau antibody K9JA (Fig. 1A) detected $Tau_{RD}\Delta K$ at Mr~14 kDa in

pro-aggregant $Tau_{RD}\Delta K$ slice cultures (Fig. 1B), not visible in slice homogenates from non-transgenic animals. Endogenous mouse Tau was apparent in 1-2 bands at M_r~50-56 kDa (Fig. 1B). The molar ratio between protein levels of exogenous $Tau_{RD}\Delta K$ and endogenous mouse Tau was ~0.8:1 (n=6 experiments, 6-8 sister slices per experiment) assuming that the antibody binds roughly equally to the repeat domain and full-length Tau (Fig. 1C). We used luciferase as a reporter co-expressed with $Tau_{RD}\Delta K$ to determine localization and strength of transgene expression in hippocampal slices (Fig. 1D). The highest activity occurred in area CA1-CA3 and pre- and/or parasubiculum whereas activity in the DG was ~three-fold lower (n=7 slices, 3 animals) (Fig. 1E). To follow transgene expression over time, bioluminescence was measured in 5-day intervals from DIV10-DIV30. Luciferase activity declined steadily to ~60% of the initial level at DIV30 ($p<0.05$; n=5 experiments, 6-8 sister slices per experiment) (Fig. 1F). $Tau_{RD}\Delta K$ expression depends on CaMKIIα-tTA which is already active in newborn mice (Krestel et al, 2001) and promotes the expression of human Tau in the absence of doxycycline (DOX). To analyze the efficiency of this switch-off system, sister slices (n=3 experiments, 3 animals) were cultured either with media alone (to allow expression of exogenous Tau) or with DOX to suppress exogenous Tau. In the presence of DOX $Tau_{RD}\Delta K$ was not detectable in western blot analysis (Fig. S1C,D). This was confirmed by strongly reduced luciferase activity already six hours after DOX application ($F_{(2/22)}=137.5$; $p<0.001$; n=8-9 experiments, 6 sister slices per experiment) (Fig. S1A,B).

3.2 Pro-aggregant $Tau_{RD}\Delta K$ causes Tau aggregation

Thioflavine S (ThS) is a common marker for insoluble protein aggregates with ß-pleated sheets. We detected ThS labeled cells in cell bodies of area CA1 and CA3 in $Tau_{RD}\Delta K$ expressing slices, starting around DIV20 (data not shown) and prominent at DIV25 (Fig. 2B,C), but absent in slice cultures from non-transgenic litter mates (Fig. 2A). Aggregates were co-stained against phosphorylation independent Tau antibody (K9JA, Fig. 2B,C) and phospho-Tau (pS396/pS404, PHF1 epitope, lying outside the repeat domain, Fig. 2C) confirming the presence of co-aggregates of human and mouse Tau. The appearance of aggregated Tau protein in $Tau_{RD}\Delta K$ slice cultures was confirmed biochemically by sarkosyl-extraction (Greenberg & Davies, 1990) followed by western blot analysis with K9JA antibodies, which detected an insoluble fraction of both exogenous and endogenous Tau in $Tau_{RD}\Delta K$ slice cultures at DIV25 (Fig. 2D, lane 3). $Tau_{RD}\Delta K$ was detected in homogenates of transgenic slices at ~14kDa (Fig. 2D, lanes 1, 3) in soluble and insoluble fractions, but not in slices from control mice (Fig. 2D, lanes 2, 4). In control slices, Tau occurred only in the soluble fraction (Fig. 2D, lane 2). In contrast, in $Tau_{RD}\Delta K$ slices a prominent part of Tau was insoluble, indicating co-aggregation of human and mouse Tau.

3.3 Pro-aggregant $Tau_{RD}\Delta K$ causes phosphorylation and mislocalization of endogenous and exogenous Tau

Phosphorylation of Tau at the KXGS-motifs in the repeat domain, particularly at Ser262, reduces its affinity to microtubules in vitro (Biernat et al, 1993) and promotes the detachment of Tau from microtubules, leading to mislocalization to the somatodendritic compartment (Thies & Mandelkow, 2007). Similar features were seen in organotypic slice cultures when $Tau_{RD}\Delta K$ was expressed, i.e. the protein became highly phosphorylated at the KXGS motifs, as seen by 12E8 antibody staining (Fig. 3B). The phosphorylation was

accompanied by mislocalization into the somata and apical dendrites (including dendritic spines) of pyramidal neurons where it colocalizes with the dendritic marker MAP2a/b (Fig. 3A), in contrast to the axonal distribution observed in control slices (Fig. 3A, Fig. S2A). Mislocalization of exogenous and endogenous Tau was already observed at DIV5 (Fig. S2B). At DIV10 Tau was clearly visible in dendritic spines (Fig. 3A) and staining of Tau in DIV25 neurons indicated dystrophic features (Adalbert et al., 2009), such as irregularly shaped cell bodies, ballooned and truncated apical dendrites (Fig. S2B). Like $Tau_{RD}\Delta K$, endogenous mouse Tau became also highly phosphorylated at the KXGS motifs in slices from pro-aggregant mice (Fig. 3B). The mislocalization and hyperphosphorylation of endogenous mouse Tau was further confirmed by staining for the proline-directed phospho-epitope PHF1, lying outside the repeat domain (Fig. 1A, Fig. 3A). In contrast, the phosphorylation at the PHF1 epitope was not seen in slice cultures from control littermates (Fig. 3A). These data argue that the expression of $Tau_{RD}\Delta K$ perturbs the kinase/phosphatase balance, leading to increased phosphorylation and mislocaliaztion of all Tau variants.

3.4 Expression of $Tau_{RD}\Delta K$ reduces dendritic spine density

Missorting of Tau into the somatodendritic compartment, including dendritic spines, is considered an early sign of neuronal degeneration (Coleman & Yao 2003). We therefore wanted to analyze the effect of pro-aggregant $Tau_{RD}\Delta K$ on dendritic spines. Spines were visualized by diolistic labeling and analyzed in apical pyramidal dendrites of area CA1 (Fig. 4A,B) after 10 and 20 DIV. In non-transgenic controls we found a typical development-related three-fold increase in spine density between DIV5 and DIV20 in pyramidal CA1 neurons (not shown), similar to rat organotypic slices (De Simoni et al, 2003). In contrast, the spine density increased only two-fold in $Tau_{RD}\Delta K$ expressing slice cultures, indicating a retardation in neuronal development. For example, at DIV10 the spine density was ~1.0 spines/µm in slices from non-transgenic littermates, but significantly reduced ($F_{(2/76)}$=14.41; $p<0.001$) to only ~0.7 spines/µm in $Tau_{RD}\Delta K$ expressing slices; at DIV20 the decrease in density was still highly significant ($F_{(2/77)}$=15.64; $p<0.001$) from ~1.4 to 1.0 spines/µm (n=20-29 neurons, 15 slices per group) (Fig. 4C). Apart from the number of spines, their morphology has a strong impact on neuronal functionality (Bourne & Harris, 2008). Therefore, spines were further classified with regard to morphology (thin, stubby and mushroom spines) using 2D/3D image analysis software (NeuronStudio; Rodriguez et al, 2008) (Fig. 4D). In pro-aggregant $Tau_{RD}\Delta K$ expressing pyramidal neurons there was a pronounced (~50%) shift from mushroom-type spines ($F_{(2/27)}$=6.426; $p<0.05$) to thin spines (n=10 neurons; 480-900 spines per group) (Fig. 4E). In contrast, the fraction of stubby spines remained unchanged (Fig. 4E). Dendritic spines in $Tau_{RD}\Delta K$ slices showed a more immature morphology than non-transgenic slices (higher proportion of thin spines, lower proportion of mushroom spines).

3.5 $Tau_{RD}\Delta K$ attenuates Ca++ dynamics

Dysregulation of intracellular Ca++ dynamics appears to play an important role in Tau mediated neurodegeneration (Furukawa et al, 2003; Zempel et al, 2010; Stoppelkamp et al, 2011). Therefore we measured intracellular Ca^{++} concentration ($[Ca^{++}]i$) in slices from pro-aggregant $Tau_{RD}\Delta K$ and control animals as the ratio of fluorescence intensities excited at 340 and 380 nm (R F340/F380) (Fig. 5A,B). Ratios were measured in the *stratum radiatum*

(s.r.), *stratum pyramidale* (s.p.) and *stratum oriens* (s.o.) of area CA3 (Fig. 5A,B). The resting [Ca^{++}]i levels were similar in control and Tau_{RD}ΔK slices (ctrl: 80.6±5.1 nM; Tau_{RD}ΔK: 80.3±4.1 nM; averaged values of the three layers), but pronounced changes became apparent after KCl-induced depolarization leading to an intracellular Ca++ elevation up to 300-350 nM (Fig. 5A, B). In s.r. and s.o. stimulation with high KCL resulted in a profound increase in intracellular Ca++ in non-transgenic control slices (227.2 ± 35% and 262.6±38% respectively); by contrast, the same stimulation evoked an increase of only 132.1± 5.6% and 162.3 ± 8.7% in Tau_{RD}ΔK slices (Fig. 5 C, D, G, H). This attenuating effect on Ca++ influx in response to strong membrane depolarization was less prominent in s.p. where somata of principal neurons are located (177.6±17.8%, control vs. 152±15.4%, Tau_{RD}ΔK, Fig. 5E,F). Under physiological conditions, depolarization induced Ca++ influx through L-type voltage gated Ca++ channels (L-VGCC) and NMDAR regulates gene expression, synaptic and homeostatic plasticity (Higley & Sabatini, 2008). To test the contribution of L-VGCCs to the depolarization induced Ca++ dynamics, we applied nifedipine (a blocker of L-VGCCs) to slices 15-20 min before and during experiments. Under these conditions, the potassium-induced increase in [Ca^{++}]i was significantly decreased in control slice cultures in s.r. and s.o. (133.8±8.3% and 124.2±4.7% resp; Fig. 5D,H). Notably, this Ca^{++} reduction was similar to the maximum response observed in Tau_{RD}ΔK expressing slices without nifedepine application. Nifedipine caused only a minor reduction of Ca++ influx in Tau_{RD}ΔK expressing slices compared to its effect in control slices (132.1±5.6% (untreated) versus 116.3±2.5% (nifedipine) in s.r., Fig. 5D). The NMDAR blocker APV had no major effect on the Ca++ influx after depolarization in either control or Tau_{RD}ΔK slices (Fig. 5D,F,H; control: averaged peak reduction of three layers of -29.1±6.7%; Tau_{RD}ΔK: -11.4±5.8%). These observations indicate that the main part of depolarization-induced Ca++ influx in our slice culture system is mediated by L-VGCC`s and that overexpression of Tau_{RD}ΔK leads to severe impairment of intracellular Ca++ dynamics. During our experiments, we found that glial cells showed a delayed Ca++ response induced by membrane depolarization, compared with neurons (data not shown). Neuron reached a peak response within 30 sec after bath application of high potassium, whereas glial cells peaked at ~1 min. This difference in Ca++ kinetics allowed us to avoid “false positive” signals from glia cells.

3.6 Pro-aggregant Tau_{RD}ΔK induces neuronal death accompanied by caspase 3 activation

To determine the effect of Tau_{RD}ΔK expression on the survival of neurons we employed the LDH cell toxicity assay. Tau_{RD}ΔK expression caused a non-significant increase (p=0.122) of 13% in LDH release at DIV15 and a significant increase of 44% ($F_{(3/19)}$ =7.736; p<0.01) at DIV20, compared with non-transgenic slice cultures (Fig. 6E). This increase in LDH release was not yet apparent at an earlier time point (DIV10, Fig. 6E). To identify hippocampal sub regions affected by the increased toxicity, NeuN positive cells were counted in area DG, CA1 and CA3 in slice cultures expressing Tau_{RD}ΔK and in control slices (8-10 slices, 6 animals per group) (Fig. 6A). The number of neurons was reduced but not significantly by ~20% in areas CA3 and CA1 at DIV20 and significantly at DIV25 (-37% in CA3, -28% in CA1; $F_{(2/30)}$=4.405; p <0.05 and $F_{(2/31)}$=5,41; p<0.05 respectively) Fig. 6C) when compared to control slices. Neuronal numbers in areas CA1 and CA3 were only slightly affected at

DIV15 (-6%). Neuronal cell death was less prominent (and not significant) in the DG (-13% at DIV25) (Fig. 6B,C). This difference is likely due to the different expression level of the transgene within the areas CA and DG (Fig. 6D). Areas CA1-3 show higher reporter gene activity compared with the DG, correlating with increased neuronal death (r=0.9759; Fig. 6D). By contrast, there was no neuronal loss in the absence of $Tau_{RD}\Delta K$ at DIV25. $Tau_{RD}\Delta K$ slice cultures switched off by doxycycline (treatment from DIV1-DIV25, n=11 slices) had equal cell numbers as control slices (100% (control) versus 98±6% (n=9 slices, 6 animals)). To test if the $Tau_{RD}\Delta K$ induced neurotoxicity occurred via the apoptotic pathway, caspase-3 activity was determined fluorimetrically, revealing a non-signifcant increase by 10% at DIV15 and by 40% ($F_{(2/16)}$=12.20; p<0.001) at DIV20 in $Tau_{RD}\Delta K$ expressing slice cultures compared with non-transgenic litter mates (n=6-7 experiments, 6 sister slices per group), (Fig. 6F) whereas caspase-3 activity was unchanged at DIV10 (Fig. 6F). In a further experiment we examined whether the presence of a caspase inhibitor can prevent the toxicity. $Tau_{RD}\Delta K$ slice cultures were treated with the caspase 3/7 inhibitor DEVD-CHO (30μM; Nicholson et al, 1995) from DIV10 to DIV20. In the presence of DEVD-CHO toxicity at DIV20 (measured via LDH release) was reduced to control levels ($F_{(2/12)}$=8.49; p<0.01) (Fig. 6F).

Neurodegeneration is closely associated with an activation of inflammatory cells in AD (Wyss-Coray, 2006; Querfurth & LaFerla, 2010). In agreement, we found high levels of activated glial cells in our slice model at DIV25 as judged by immunohistochemistry stainings against microglia (Fig. S3A), astrocytes (data not shown) in all hippocampal subregions and the presence of reactive oxygen species (ROS) (Fig. S3B/C). Slice cultures prepared from $Tau_{RD}\Delta K$ mice showed a higher number of activated microglia at DIV25 (Fig. S3A) and an increased production of ROS (Fig. S3C) when compared to control slices.

3.7 Pathological effects of $Tau_{RD}\Delta K$ are prevented by aggregation inhibitors

Throughout these experiments, we asked whether the negative effects of pro-aggregant $Tau_{RD}\Delta K$ expression could be prevented or reversed by inhibiting aggregation. As an example, we tested compound bb14, one of the inhibitors from the rhodanine class (Fig. 2E) identified in a screen for Tau aggregation inhibitors (Pickhardt et al, 2005; Bulic et al, 2007). Treatment of $Tau_{RD}\Delta K$ slices with 15 μM bb14 reduced the fraction of sarkosyl-insoluble exogenous Tau significantly by ~70% in comparison to untreated $Tau_{RD}\Delta K$ slices (p<0.001; n=4 experiments; ~50 slices, 5 animals per experiment) (Fig. 2F), and reduced the phosphorylation at S262/S356 of endogenous mouse Tau (-40%) and particularly of exogenous $Tau_{RD}\Delta K$ (-80%; p<0.001, n=3) (Fig. 3C,D). Mislocalization of Tau into the somatodendritic compartment was also observed in bb14 treated slice cultures (Fig. S2C) but without dystrophic features. Compound bb14 partly rescued spine toxicity observed in $Tau_{RD}\Delta K$ slices at both time points investigated ($F_{(2/76)}$=14.41; p<0.01 (DIV10) and $F_{(2/77)}$=15.64; p<0.05 (DIV20)) in comparison with control slices (Fig. 4B,C), and partly prevented conversion to “immature” spine morphology due to $Tau_{RD}\Delta K$ expression (Fig. 4E). The fraction of mushroom spines returned nearly to control levels, and thin spines were partly reduced. Correspondingly, the impairment in the Ca++ influx after depolarization was rescued in bb14 treated cultures in all three layers (Fig. 5D,F,H). The most prominent beneficial effect was observed in *stratum radiatum* (88.7± 28.8% (treated) versus

32.1± 5.6% (untreated)) and compared to control slices. Finally, neurotoxicity was prevented by bb14 in all hippocampal subregions (Fig. 6B,C). Neuronal numbers in bb14-treated $Tau_{RD}\Delta K$ slices remained equal to those in control slices (Fig. 6C). The protective effect on toxicity of bb14 was confirmed by a pronounced decrease in LDH release in $Tau_{RD}\Delta K$ slices nearly to control levels (Fig. 6E) as well as reduced caspase 3 activities (Fig. 6F). The inflammatory response at DIV25 was reduced in parallel (Fig. S3C).

4 Discussion

The role of Tau under normal and pathological conditions is still poorly understood. In order to make advancements in understanding one needs fast, flexible and robust test systems. The aim of this study was to generate a tauopathy model which makes the pathological cascade accessible to experimental intervention and analysis and allows testing of aggregation inhibitors. By using organotypic hippocampal slices, which maintain many aspects of in vivo biology (Gahwiler, 1988), we could recapitulate major aspects of tauopathy and demonstrate the neuroprotective capacity of aggregation inhibitors.

In mature neurons, Tau is mostly axonal (Binder et al, 1985), although dendritic functions have been proposed as well (Ittner et al, 2010; Morris et al, 2011). In our control slices mouse Tau was restricted to axons, whereas in slices from pro-aggregant $Tau_{RD}\Delta K$ mice exogenous and endogenous Tau was mislocalized to cell bodies, dendrites and dendritic spines. For endogenous Tau, the appearance in the somatodendritic compartment is unexpected and indicates that pro-aggregant $Tau_{RD}\Delta K$ expression forces also endogenous mouse Tau to mislocalize starting at DIV5. Mislocalization of exogenous and endogenous mouse Tau is closely correlated with phosphorylation at S262/S356 which reduces Tau's affinity for microtubules (Drewes et al, 1997; Thies & Mandelkow, 2007).

In mice, the co-aggregation of exogenous and endogenous Tau becomes detectable at advanced age (Mocanu et al, 2008). We confirmed this finding for the slice model, but in this case it occurred on a much shorter time scale (weeks rather than months as in transgenic mice. This acceleration of pathological changes in cultured slices compared with transgenic mice was also observed for other pathological features, including Tau missorting, synaptotoxicity and cell death (compare Fig. 7 with Sydow et al, 2011). Since the organotypic slice model allows easy experimental access it was possible to observe other features as well, for example the increase in caspase 3 activity parallel to an increased LDH release due to $Tau_{RD}\Delta K$ expression. On the basis of these oberservations we infer that apoptotic processes contribute strongly to neuronal cell death in our model. However, whether or not this represents the situation in human conditions is still a matter of debate (Spires-Jones et al, 2011). Besides neurotoxicity, it was possible to investigate synaptotoxicity in the slice model in terms of morphological spine changes and final spine loss. Mislocalized Tau was already present in dendritic spines at an early time point, similar to observations in primary neuronal cell culture (Thies et al, 2007; Zempel et al, 2010; Hoover et al, 2010). Density and dynamics of dendritic spines is thought to be a structural correlate of synaptic strength and plasticity (Bonhoeffer & Yuste, 2002). In particular, the number of voltage gated Ca^{++} channels (VGCCs) increases with greater spine volume, thereby enhancing Ca^{++} influx (Sabatini & Svoboda, 2000). The loss of dendritic spines and

their morphological modulation from mushroom-shaped to thin spines in pro-aggregant $Tau_{RD}\Delta K$ slices was reflected in functional constraints measured by Ca^{++} imaging. The main source of activity-related Ca^{++} influx was mediated by L-VGCCs and NMDA receptors, which are both present in dendritic spines (Higley & Sabatini, 2008). The Ca^{++} influx after a depolarizing stimulus was strongly decreased in $Tau_{RD}\Delta K$ slices. Since we observed a reduced sensitivity to the L-VGCC blocker nifedepine in $Tau_{RD}\Delta K$ slices compared to controls we suspect a $Tau_{RD}\Delta K$ specific impairment in Ca^{++} dynamics through L-VGCCs. Correspondingly, the reduction in Ca++ influx in $Tau_{RD}\Delta K$ slices could be mimicked in control slices by treating them with the L-VGCC blocker nifedepine. In our model the loss of dendritic spines and the shift from mushroom-shaped to thin spines could thus contribute to the observed Ca++ impairment. Considering that the proline-rich region of Tau has a high affinity for proteins with src homology 3 (SH3) domains (Reynolds et al., 2008) one could speculate that mislocalized mouse Tau might contribute to the impairment of Ca++ dynamics by a direct interaction with the SH3 domain of the ß-subunit of L-VGCC. In any case, since the funtional impairment of Ca++ dynamics in $Tau_{RD}\Delta K$ slices occurs before neurofibrillary tangle formation, it is likely that Tau monomers or oligomeric species are responsible for early functional deficits in depolarization evoked Ca++ responses.

Given that Tau aggregation is closely related to the Alzheimer disease process, the inhibition of Tau aggregation is a promising therapeutic target. Therefore, one aim of this study was to test aggregation inhibitors in a more physiological paradigm than previous cell culture based systems (Pickhardt et al, 2005). Results with the rhodanine-based compound bb14 (Bulic et al, 2007) demonstrate the feasibility of this approach. Treatment of slices with compound bb14 inhibited Tau aggregation and partly prevented the loss of spines and neurons, arguing that pathological changes are closely related to Tau's aggregation/oligomerization process.

The importance of the capacity of Tau to aggregate for the development of pathology was supported by previous findings with an another transgenic mouse line expressing the same construct with additional proline mutations (anti-aggregant $Tau_{RD}\Delta K280PP$; Mocanu et al, 2008). This mouse line developed no phenotype typical for tauopathies, indicating that ß-propensity is central to the pathology. In contrast to previous slice models of tauopathy (Duff et al, 2002; Congdon et al, 2009), we could model the whole range of pathological aspects and thereby analyze their exact chronology (for a summary see Fig. 7) without side effects due to viral vectors in transiently expressing models (Shahani et al, 2006; Hinners et al, 2008). Our study demonstrates the neuroprotective effect of bb14 and the potential pathogenic effects of Tau on L-VGCCs. Therefore, this model lends itself to the evaluation of pathological processes and different Tau aggregation inhibitors, which is currently in progress.

Supporting information

Refer to Web version on PubMed Central for supplementary material.

Acknowledgements

We are grateful to Dr. A. Sydow and Dr. K. Hochgräfe for expert help with transgenic mice, A. Hofmann and Y. Biederbeck for help with mouse breeding, Dr. A. Marx for advice on statistics, Dr. J. Biernat for valuable

suggestions on this manuscript. We gratefully acknowledge reagents from Dr. E. Kandel (Columbia University, New York, NY; CaMKIIα-tTA activator transgenic mice), Dr. P. Seubert (Elan Pharma, South San Francisco, CA; 12E8 antibody), and Dr. P. Davies (Albert Einstein College, Bronx, NY; PHF-1 antibodies), Dr. Marcus Pickhardt and Dr. B. Bulic (CAESAR, Bonn) for providing aggregation inhibitor compound bb14. We thank Dr. A. Haemisch and his team at the animal facility at Hamburg University Medical School for their efficient support. This work was supported by the Max Planck Society, DZNE, EU-FP7/Memosad, Metlife Foundation, BMBF (KNDD Project), and Wellcome Trust/MRC.

Abbreviations

AD	Alzheimer Disease
CA1	cornu ammonis 1
CA3	cornu ammonis 3
CaMKIIα	calcium/calmodulin-dependent protein kinase IIα
Casp3	caspase 3
C-terminal	Carboxy-terminus
[Ca^{++}]i	intracellular calcium concentration
DG	dentate gyrus
DIV	Days *in vitro*
DOX	doxycycline
FTDP-17	Frontotemporal dementia and parkinsonism linked to chromosome17
LDH	lactate dehydrogenase
LUC	Firefly luciferase
L-VGCC	L-type voltage gated calcium channel
MAPs	Microtubules associated proteins
NeuN	neuronal nuclear protein
NMDAR	NMDA-type glutamate receptor
PHF	paired helical filament
RT	room temperature
Tau_{RD}ΔK, TΔK	Tau repeat domain with FTDP-17 mutation ΔK280

References

Adalbert R, Nogradi A, Babetto E, Janeckova L, Walker SA, Kerschensteiner M, Misgeld T, Coleman MP. Severely dystrophic axons at amyloid plaques remain continuous and connected to viable cell bodies. Brain. 2009; 132:402–416. [PubMed: 19059977]

Europe PMC Funders Author Manuscripts

Ballatore C, Lee VM, Trojanowski JQ. Tau-mediated neurodegeneration in Alzheimer's disease and related disorders. Nat Rev Neurosci. 2007; 8:663–672. [PubMed: 17684513]

Barghorn S, Zheng-Fischhofer Q, Ackmann M, Biernat J, von Bergen M, Mandelkow EM, Mandelkow E. Structure, microtubule interactions, and paired helical filament aggregation by tau mutants of frontotemporal dementias. Biochemistry. 2000; 39:11714–11721. [PubMed: 10995239]

Biernat J, Gustke N, Drewes G, Mandelkow EM, Mandelkow E. Phosphorylation of Ser262 strongly reduces binding of tau to microtubules: distinction between PHF-like immunoreactivity and microtubule binding. Neuron. 1993; 11:153–163. [PubMed: 8393323]

Binder LI, Frankfurter A, Rebhun LI. The distribution of tau in the mammalian central nervous system. J Cell Biol. 1985; 101:1371–1378. [PubMed: 3930508]

Bonhoeffer T, Yuste R. Spine motility. Phenomenology, mechanisms, and function. Neuron. 2002; 35:1019–27. [PubMed: 12354393]

Braak H, Braak E. Neuropathological stageing of Alzheimer-related changes. Acta Neuropathol. 1991; 82:239–259. [PubMed: 1759558]

Braak H, Braak E. Morphological criteria for the recognition of Alzheimer's disease and the distribution pattern of cortical changes related to this disorder. Neurobiol Aging. 1994; 15:355–356. discussion 379-380. [PubMed: 7936061]

Bonhoeffer T, Yuste R. Spine motility. Phenomenology, mechanisms, and function. Neuron. 2002; 35:1019–27. [PubMed: 12354393]

Bulic B, Pickhardt M, Khlistunova I, Biernat J, Mandelkow EM, Mandelkow E, Waldmann H. Rhodanine-based tau aggregation inhibitors in cell models of tauopathy. Angew Chem Int Ed Engl. 2007; 46:9215–9219. [PubMed: 17985339]

Coleman PD, Yao PJ. Synaptic slaughter in Alzheimer's disease. Neurobiol Aging. 2003; 24:1023–1027. [PubMed: 14643374]

Congdon EE, Figueroa YH, Wang L, Toneva G, Chang E, Kuret J, Conrad C, Duff KE. Inhibition of tau polymerization with a cyanine dye in two distinct model systems. J Biol Chem. 2009; 284:20830–20839. [PubMed: 19478088]

Contag CH. In vivo pathology: seeing with molecular specificity and cellular resolution in the living body. Annu Rev Pathol. 2007; 2:277–305. [PubMed: 18039101]

de Calignon A, Fox LM, Pitstick R, Carlson GA, Bacskai BJ, Spires-Jones TL, Hyman BT. Caspase activation precedes and leads to tangles. Nature. 2010; 464:1201–1204. [PubMed: 20357768]

De Simoni A, Griesinger CB, Edwards FA. Development of rat CA1 neurones in acute versus organotypic slices: role of experience in synaptic morphology and activity. J Physiol. 2003; 550:135–147. [PubMed: 12879864]

Drewes G, Trinczek B, Illenberger S, Biernat J, Schmitt-Ulms G, Meyer HE, Mandelkow EM, Mandelkow E. Microtubule-associated protein/microtubule affinity-regulating kinase (p110mark). A novel protein kinase that regulates tau-microtubule interactions and dynamic instability by phosphorylation at the Alzheimer-specific site serine 262. J Biol Chem. 1995; 270:7679–7688. [PubMed: 7706316]

Duff K, Noble W, Gaynor K, Matsuoka Y. Organotypic slice cultures from transgenic mice as disease model systems. J Mol Neurosci. 2002; 19:317–20. [PubMed: 12540058]

Furukawa K, Wang Y, Yao PJ, Fu W, Mattson MP, Itoyama Y, Onodera H, D'Souza I, Poorkaj PH, Bird TD, et al. Alteration in Ca++ channel properties is responsible for the neurotoxic action of a familial frontotemporal dementia tau mutation. J Neurochem. 2003; 87:427–436. [PubMed: 14511120]

Gahwiler BH. Organotypic cultures of neural tissue. Trends Neurosci. 1988; 11:484–489. [PubMed: 2469173]

Gamblin TC, Chen F, Zambrano A, Abraha A, Lagalwar S, Guillozet AL, Lu M, Fu Y, Garcia-Sierra F, LaPointe N, Miller R, et al. Caspase cleavage of tau: linking amyloid and neurofibrillary tangles in Alzheimer's disease. Proc Natl Acad Sci U S A. 2003; 100:10032–10037. [PubMed: 12888622]

Giannakopoulos P, Herrmann FR, Bussiere T, Bouras C, Kovari E, Perl DP, Morrison JH, Gold G, Hof PR. Tangle and neuron numbers, but not amyloid load, predict cognitive status in Alzheimer's disease. Neurology. 2003; 60:1495–1500. [PubMed: 12743238]

Gomez-Isla T, Hollister R, West H, Mui S, Growdon JH, Petersen RC, Parisi JE, Hyman BT. Neuronal loss correlates with but exceeds neurofibrillary tangles in Alzheimer's disease. Ann Neurol. 1997; 41:17–24. [PubMed: 9005861]

Greenberg SG, Davies P. A preparation of Alzheimer paired helical filaments that displays distinct tau proteins by polyacrylamide gel electrophoresis. Proc Natl Acad Sci U S A. 1990; 87:5827–5831. [PubMed: 2116006]

Grynkiewicz G, Poenie M, Tsien RY. A new generation of Ca2+ indicators with greatly improved fluorescence properties. J Biol Chem. 1985; 260:3440–3450. [PubMed: 3838314]

Higley MJ, Sabatini BL. Calcium signaling in dendrites and spines: practical and functional considerations. Neuron. 2008; 59:902–913. [PubMed: 18817730]

Hinners I, Hill A, Otto U, Michalsky A, Mack TG, Striggow F. Tau kinase inhibitors protect hippocampal synapses despite of insoluble tau accumulation. Mol Cell Neurosci. 2008; 37:559–567. [PubMed: 18201898]

Hoover BR, Reed MN, Su J, Penrod RD, Kotilinek LA, Grant MK, Pitstick R, Carlson GA, Lanier LM, Yuan LL, Ashe KH, et al. Tau mislocalization to dendritic spines mediates synaptic dysfunction independently of neurodegeneration. Neuron. 2010; 68:1067–81. [PubMed: 21172610]

Ittner LM, Ke YD, Delerue F, BI M, Gladbach A, Van Eersel J, Wolfing H, Chieng BC, Christie MJ, Napier IA, Eckert A, et al. Dendritic function of tau mediates amyloid-beta toxicity in Alzheimer's disease mouse models. Cell. 2010; 142:387–97. [PubMed: 20655099]

Khlistunova I, Biernat J, Wang Y, Pickhardt M, von Bergen M, Gazova Z, Mandelkow E, Mandelkow EM. Inducible expression of Tau repeat domain in cell models of tauopathy: aggregation is toxic to cells but can be reversed by inhibitor drugs. J Biol Chem. 2006; 281:1205–1214. [PubMed: 16246844]

Krestel HE, Mayford M, Seeburg PH, Sprengel R. A GFP-equipped bidirectional expression module well suited for monitoring tetracycline-regulated gene expression in mouse. Nuc Acids Res. 2001; 29:E39.

Mayford M, Baranes D, Podsypanina K, Kandel ER. The 3'-untranslated region of CaMKII alpha is a cis-acting signal for the localization and translation of mRNA in dendrites. Proc Natl Acad Sci U S A. 1996; 93:13250–13255. [PubMed: 8917577]

Mocanu M, Nissen A, Eckermann K, Khlistunova I, Biernat J, Drexler D, Petrova O, Schonig K, Bujard H, Mandelkow E, Zhou L, et al. The potential for beta-structure in the repeat domain of tau protein determines aggregation, synaptic decay, neuronal loss, and coassembly with endogenous Tau in inducible mouse models of tauopathy. J Neurosci. 2008; 28:737–748. [PubMed: 18199773]

Moolman DL, Vitolo OV, Vonsattel JP, Shelanski ML. Dendrite and dendritic spine alterations in Alzheimer models. J Neurocytol. 2004; 33:377–387. [PubMed: 15475691]

Morris M, Maeda S, Vossel K, Mucke L. The many faces of tau. Neuron. 2011; 70:410–26. [PubMed: 21555069]

Nicholson DW, Ali A, Thornberry NA, Vaillancourt JP, Ding CK, Gallant M, Gareau Y, Griffin PR, Labelle M, Lazebnik YA, et al. Identification and inhibition of the ICE/CED-3 protease necessary for mammalian apoptosis. Nature. 1995; 376:37–43. [PubMed: 7596430]

Pickhardt M, Von Bergen M, Gazova Z, Hascher A, Biernat J, Mandelkow EM, Mandelkow E. Screening for inhibitors of tau polymerization. Curr Alzheimer Res. 2005; 2:219–26. [PubMed: 15974921]

Querfurth HW, Laferla FM. Alzheimer's disease. N Engl J Med. 2010; 362:329–44. [PubMed: 20107219]

Reynolds CH, Garwood CJ, Wray S, Price C, Kellie S, Perera T, Zvelebil M, Yang A, Sheppard PW, Varndell IM, Hanger DP, et al. Phosphorylation regulates tau interactions with Src homology 3 domains of phosphatidylinositol 3-kinase, phospholipase Cgamma1, Grb2, and Src family kinases. J Biol Chem. 2008; 283:18177–18186. [PubMed: 18467332]

Rizzu P, Van Swieten JC, Joosse M, Hasegawa M, Stevens M, Tibben A, Niermeijer MF, Hillebrand M, Ravid R, Oostra BA, Goedert M, et al. High prevalence of mutations in the microtubule-associated protein tau in a population study of frontotemporal dementia in the Netherlands. Am J Hum Genet. 1999; 64:414–421. [PubMed: 9973279]

Rodriguez A, Ehlenberger DB, Dickstein DL, Hof PR, Wearne SL. Automated three-dimensional detection and shape classification of dendritic spines from fluorescence microscopy images. PLoS One. 2008; 3:e1997. [PubMed: 18431482]

Rohn TT, Rissman RA, Davis MC, Kim YE, Cotman CW, Head E. Caspase-9 activation and caspase cleavage of tau in the Alzheimer's disease brain. Neurobiol Dis. 2002; 11:341–354. [PubMed: 12505426]

Sabatini BL, Svoboda K. Analysis of calcium channels in single spines using optical fluctuation analysis. Nature. 2000; 408:589–593. [PubMed: 11117746]

Shahani N, Subramaniam S, Wolf T, Tackenberg C, Brandt R. Tau aggregation and progressive neuronal degeneration in the absence of changes in spine density and morphology after targeted expression of Alzheimer's disease-relevant tau constructs in organotypic hippocampal slices. J Neurosci. 2006; 26:6103–6114. [PubMed: 16738255]

Smith DL, Pozueta J, Gong B, Arancio O, Shelanski M. Reversal of long-term dendritic spine alterations in Alzheimer disease models. Proc Natl Acad Sci U S A. 2009; 106:16877–16882. [PubMed: 19805389]

Spires-Jones TL, Kopeikina KJ, Koffie RM, de Calignon A, Hyman BT. Are Tangles as Toxic as They Look? J Mol Neurosci. 2011 [Epub].

Stoppelkamp S, Bell HS, Palacios-Filardo J, Shewan DA, Riedel G, Platt B. In vitro modelling of Alzheimer's disease: degeneration and cell death induced by viral delivery of amyloid and tau. Exp Neurol. 2011; 229:226–237. [PubMed: 21295028]

Stoppini L, Buchs PA, Muller D. A simple method for organotypic cultures of nervous tissue. J Neurosci Methods. 1991; 37:173–182. [PubMed: 1715499]

Sydow A, Van Der Jeugd A, Zheng F, Ahmed T, Balschun D, Petrova O, Drexler D, Zhou L, Rune G, Mandelkow E, D'hooge R, et al. Tau-induced defects in synaptic plasticity, learning, and memory are reversible in transgenic mice after switching off the toxic tau mutant. J Neurosci. 2011; 31:2511–25. [PubMed: 21325519]

Thies E, Mandelkow EM. Missorting of tau in neurons causes degeneration of synapses that can be rescued by the kinase MARK2/Par-1. J Neurosci. 2007; 27:2896–2907. [PubMed: 17360912]

von Bergen M, Friedhoff P, Biernat J, Heberle J, Mandelkow EM, Mandelkow E. Assembly of tau protein into Alzheimer paired helical filaments depends on a local sequence motif ((306)VQIVYK(311)) forming beta structure. Proc Natl Acad Sci U S A. 2000; 97:5129–5134. [PubMed: 10805776]

Wyss-Coray T. Inflammation in Alzheimer disease: driving force, bystander or beneficial response? Nat Med. 2006; 12(9):1005–15. [PubMed: 16960575]

Zempel H, Thies E, Mandelkow E, Mandelkow EM. Abeta oligomers cause localized Ca(2+) elevation, missorting of endogenous Tau into dendrites, Tau phosphorylation, and destruction of microtubules and spines. J Neurosci. 2010; 30:11938–11950. [PubMed: 20826658]

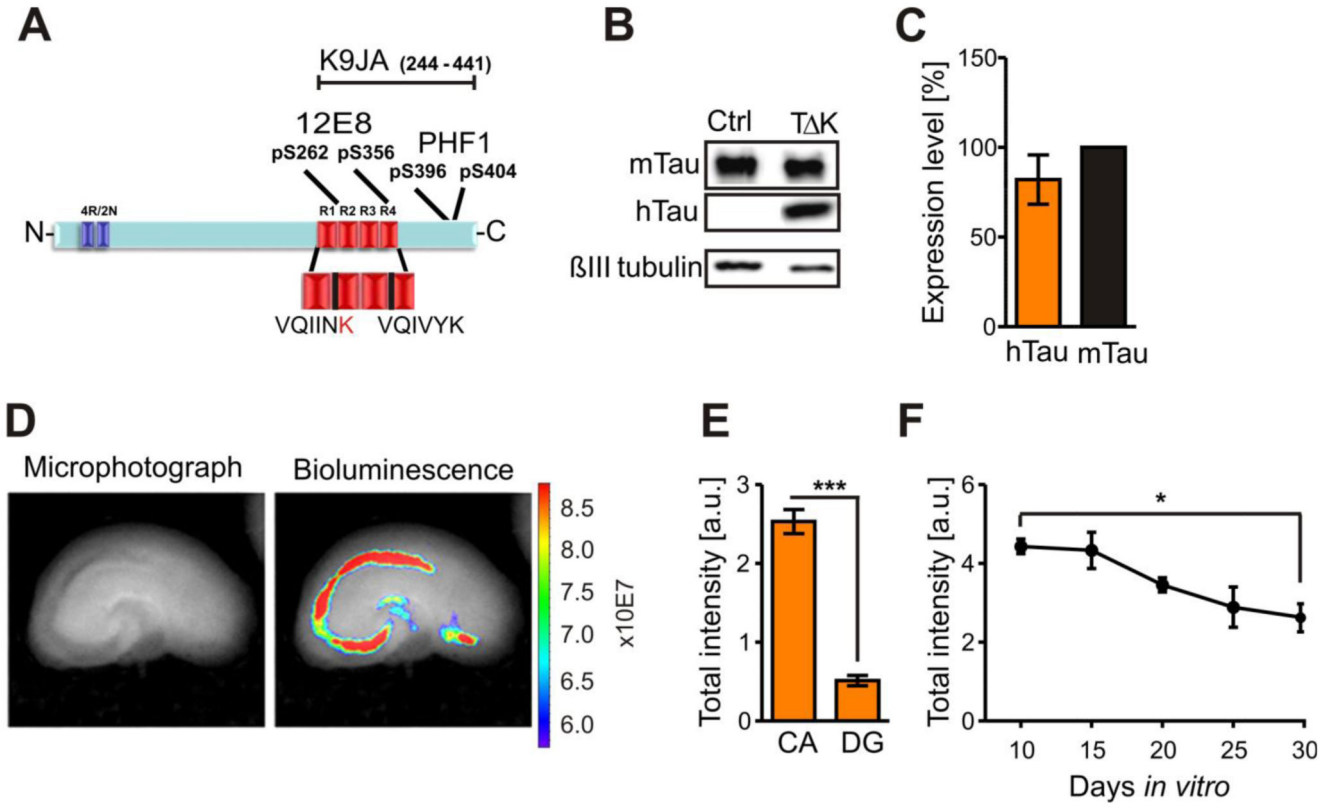

Fig. 1. Human Tau_{RD}ΔK is highly expressed in area CA1 and CA3 in slice cultures.

(A) Tau_{RD}ΔK construct is based on the human Tau repeat domain carrying the FTDP-17 mutation ΔK280. Four repeats in the C-terminal half of Tau are highlighted in red (R1-R4). The sequence of the two hexapeptide motifs at beginning of R2 and R3, which promote aggregation by inducing ß-structure, is shown. The FTDP-17 mutation ΔK280 within R2 (marked in red) strongly increase the propensity for ß-structure. Epitopes recognized by phosphorylation-dependent antibodies 12E8 and PHF1 and pan-Tau antibody K9JA are indicated.

(B) Slice homogenates of either control or Tau_{RD}ΔK cultures were blotted with the Tau antibody K9JA. Endogenous mouse Tau is detected at ~56kDa and Tau_{RD}ΔKat ~14kDa.

(C) Molar ratio of exogenous Tau_{RD}ΔKto endogenous mouse Tau is ~0.8:1 (n=6 experiments (6-8 sister slices/group, 6 animals)).

(D) Luciferase activity within Tau_{RD}ΔK slices (DIV5) were determined by bioluminescence (photons/sec) in area CA and DG (bright field image; left panel). Luciferase activity (right panel) is very high in the CA region and in the remaining cells of the cortex.

(E) Quantification of the luciferase activities in CA and DG region. Area CA1-3 show ~three-fold higher activities (n = 7 slices, 3 animals, *Unpaired t-test *** p- value < 0.001*).

(F) Luciferase activity monitored over 20 days *in vitro*. The signal is constant up to 15 DIV but declines thereafter to ~60% of its maximum value at DIV10 (n = 5 experiments, 6 slices/ experiment, 3 animals, *Unpaired t-test * p- value < 0.05*).

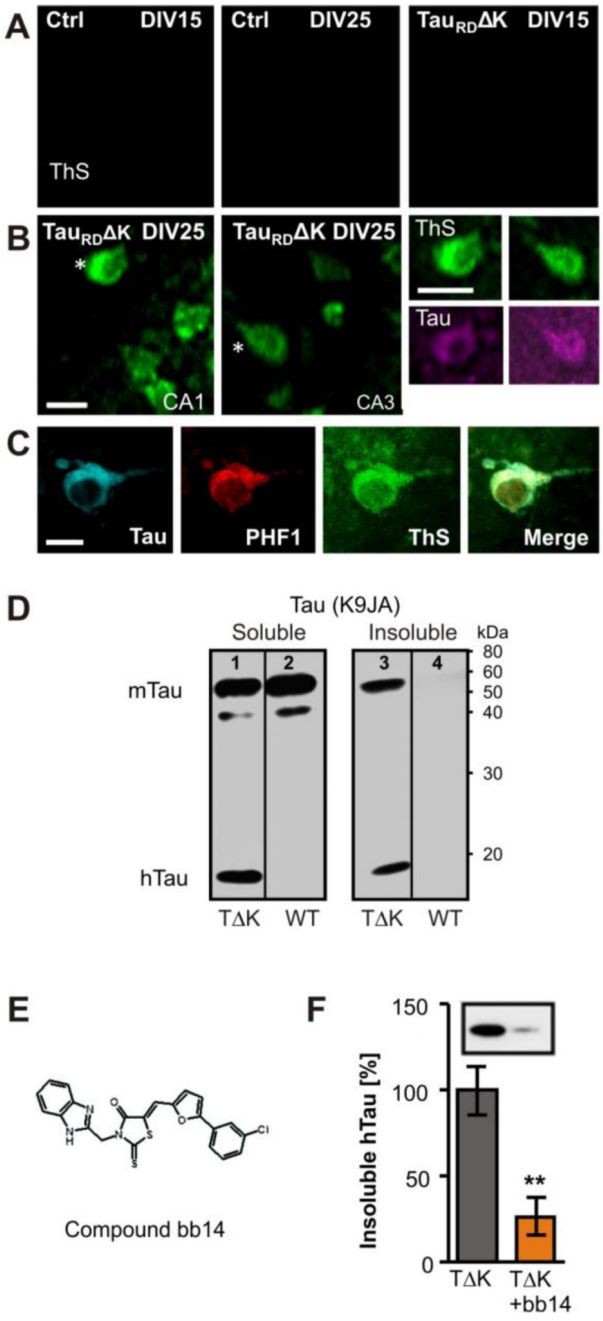

Fig. 2. Expression of Tau_{RD}ΔK causes Tau aggregation in the CA region.

(A) Tau_{RD}ΔK or control slices were stained with thioflavine S (ThS) after 15 or 25 days in vitro Control slices showed no ThS signal after 15 or 25 DIV.

(B,C) Tau_{RD}ΔK slices developed Tau aggregates at DIV 25 but not before. Aggregates appeared inside the somata and could also be stained with K9JA Tau antibodies (asterisks). The co-aggregation of human and mouse Tau was confirmed by antibodies specific for phosphorylated mouse Tau at pS396/pS404 (PHF1).

(D) Western blotting of the soluble (lanes 1, 2) and sarkosyl-insoluble (lanes 3, 4) fraction with K9JA antibodies of DIV25 slices. Human $Tau_{RD}\Delta K$ is detected in homogenates of transgenic slices as a prominent band at Mr ~14kDa in both the soluble (lane 1) and insoluble fractions (lane 3), but not in slices from control mice (lanes 2, 4). In control slices, endogenous mouse Tau occurs only in the soluble fraction. In contrast, in $Tau_{RD}\Delta K$ slices a prominent part of mouse Tau was insoluble, indicating co-aggregation of endogenous and exogenous Tau (lane 3).

(E) Structure of compound bb14, a rhodanine-based tau aggregation inhibitor (Bulic et al, 2007).

(F) Influence of compound bb14 on the aggregation of Tau was investigated by densitometry after western blot analysis with K9JA Tau antibodies of the sarkosyl-insoluble Tau fraction. Compound bb14 (15 μM, treated DIV1-DIV25) reduced the fraction of insoluble $Tau_{RD}\Delta K$ by ~70% (n=4 experiments, *unpaired t-test ** p- value < 0.01*). Scale bars: **A, B**, 10μm; **C**, 5μm.

Europe PMC Funders Author Manuscripts

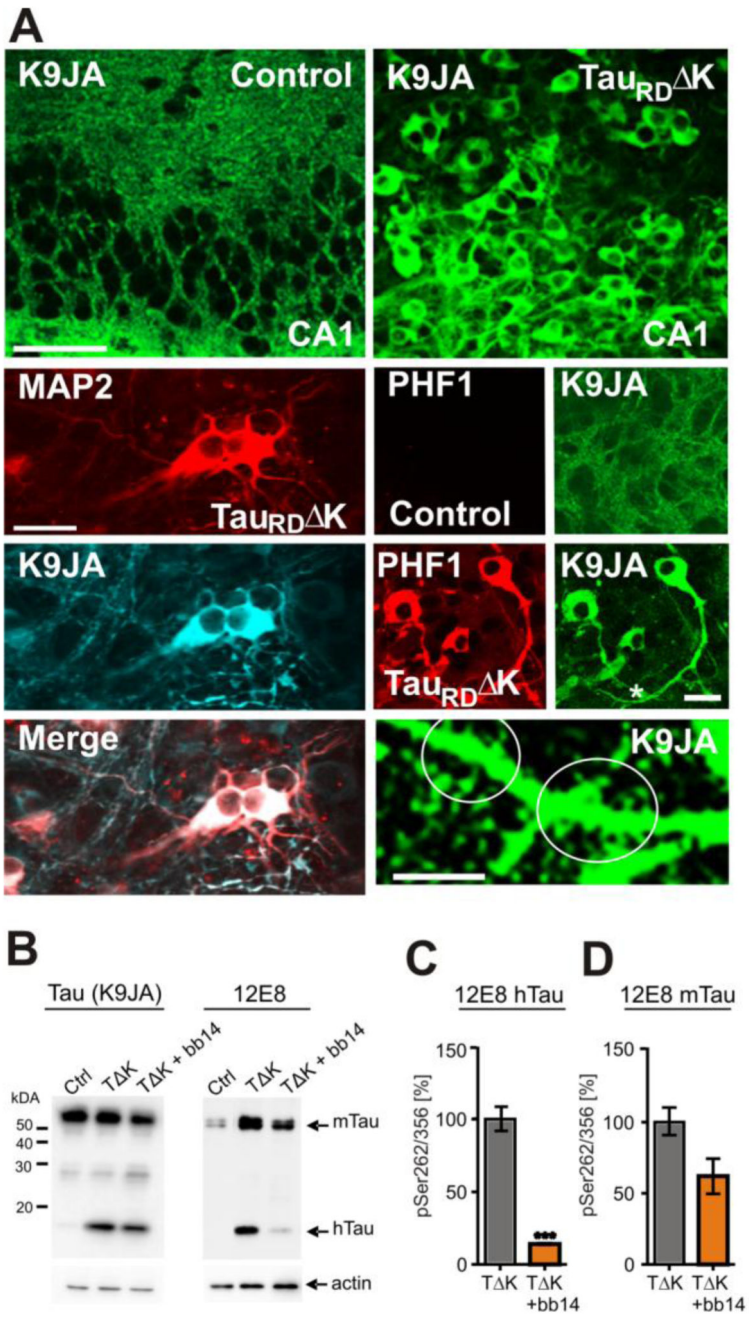

Fig. 3. Endogenous mouse Tau is phosphorylated at 12E8 and PHF1 epitopes and is mislocalized into the somatodendritic compartment.

(A) Immunoreactivity with K9JA antibodies. Microphotographs of control slice cultures indicate an axonal distribution of endogenous mouse Tau at DIV10. In contrast, pro-aggregant $Tau_{RD}\Delta K$ becomes mislocalized into somata, dendrites, where it colocalizes with the dendritic marker MAP2, and dendritic spines (white circles) in the presence of pro-aggregant $Tau_{RD}\Delta K$. Mislocalized Tau was also detected by the PHF1 antibody in $Tau_{RD}\Delta K$

slice cultures but not in slices from control littermates, confirming the presence of mislocalized endogenous mouse Tau in dendrites and soma.

(B) Western blot showing that both $Tau_{RD}\Delta K$ and endogenous Tau is highly phosphorylated at the 12E8 epitope at DIV10. The phosphorylation level of human and mouse Tau in untreated $Tau_{RD}\Delta K$ slices is higher than in control slices or in $Tau_{RD}\Delta K$ slices treated with the aggregation inhibitor bb14 from DIV1-DIV10.

(C,D) Phosphorylation at Ser262/356 of human (**C**) and mouse Tau (**D**) was reduced in samples treated with compound bb14 (by ~80% for exogenous Tau and by ~40% for endogenous Tau) (n=3 experiments; 3 animals, *unpaired t-test *** p- value < 0.001).* Scale bars in **A**, upper panel, 50μm; lower panel, 20μm; image on spines, 10μm.

Europe PMC Funders Author Manuscripts

Europe PMC Funders Author Manuscripts

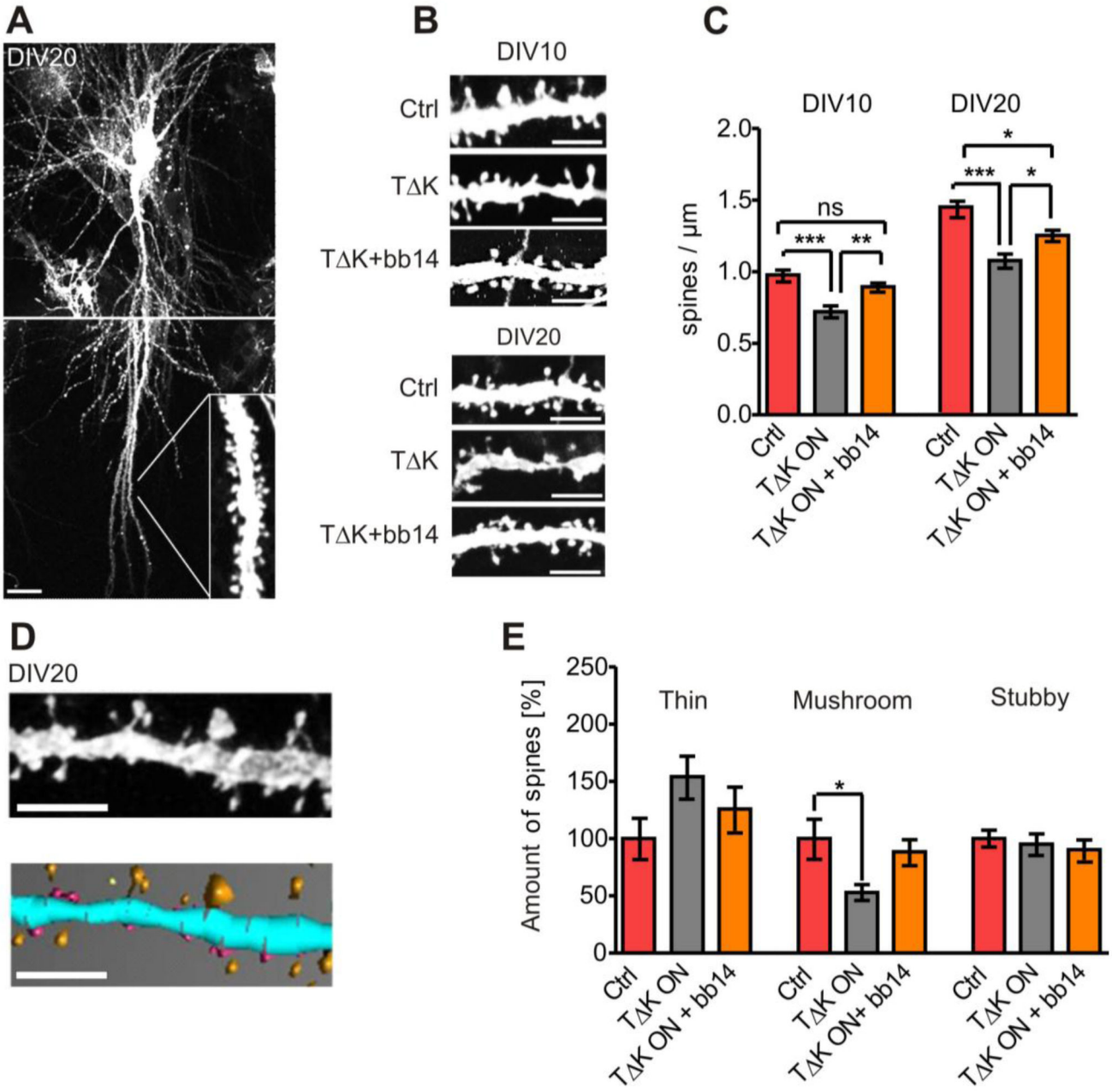

Fig. 4. Expression of Tau_{RD}ΔK causes a reduction and morphological changes of dendritic spines.

(A) Representative pyramidal neuron of area CA1 in DIV20 slice cultures visualized by diolistic labeling. The apical dendritic area taken for spine quantification is indicated.

(B) Representative apical dendritic areas of neurons (DIV10 or DIV20) are presented either in control, Tau_{RD}ΔK, and Tau_{RD}ΔK+ bb14 slices.

(C) When comparing the spine density in control, Tau_{RD}ΔK and Tau_{RD}ΔK +bb14 slices (n=25 neurons, 15 slices, 3 animals/group) quantitatively, it displays a ~25% reduction due to the presence of Tau_{RD}ΔK (DIV10 and DIV20). Treatment with compound bb14 (starting at DIV1) strongly attenuates the spine loss (decrease only -11% (DIV10) or -13% (DIV20).

*One-way ANOVA followed by Tukey's post-hoc test *** p- value < 0.001; ** p-value < 0.01; *p-value <0,05.*

(D) Apical dendritic areas in CA1 were reconstructed using NeuronStudio (Rodriguez et al, 2008). Unprocessed dendritic area (top) and representative 3D reconstruction (down). Spines were classified into thin (yellow), stubby (purple) and mushroom spines (orange) (n= 10 neurons (480-900 spines per group)) in DIV20 slices.

(E) Mushroom spines are reduced by ~50% in $Tau_{RD}\Delta K$ expressing pyramidal neurons ($F_{(2/27)}$=6.426; p<0.05). Treatment with compound bb14 (15 μM) partly abolished this reduction in mushroom spines. The fraction of thin spines increases by ~50% (p=0.139) due to $Tau_{RD}\Delta K$ expression, indicating a shift from mushroom-shaped to thin spines. Treatment with compound bb14 nearly abolishes this effect. The fraction of stubby spines is unchanged in all groups; and treatment with bb14 has no effect. *One-way ANOVA* followed by Tukey's post-hoc test ** p- value < 0.05.* Scale bars: **A**, 20μm; **B**,**D**, 5μm.

Europe PMC Funders Author Manuscripts

Europe PMC Funders Author Manuscripts

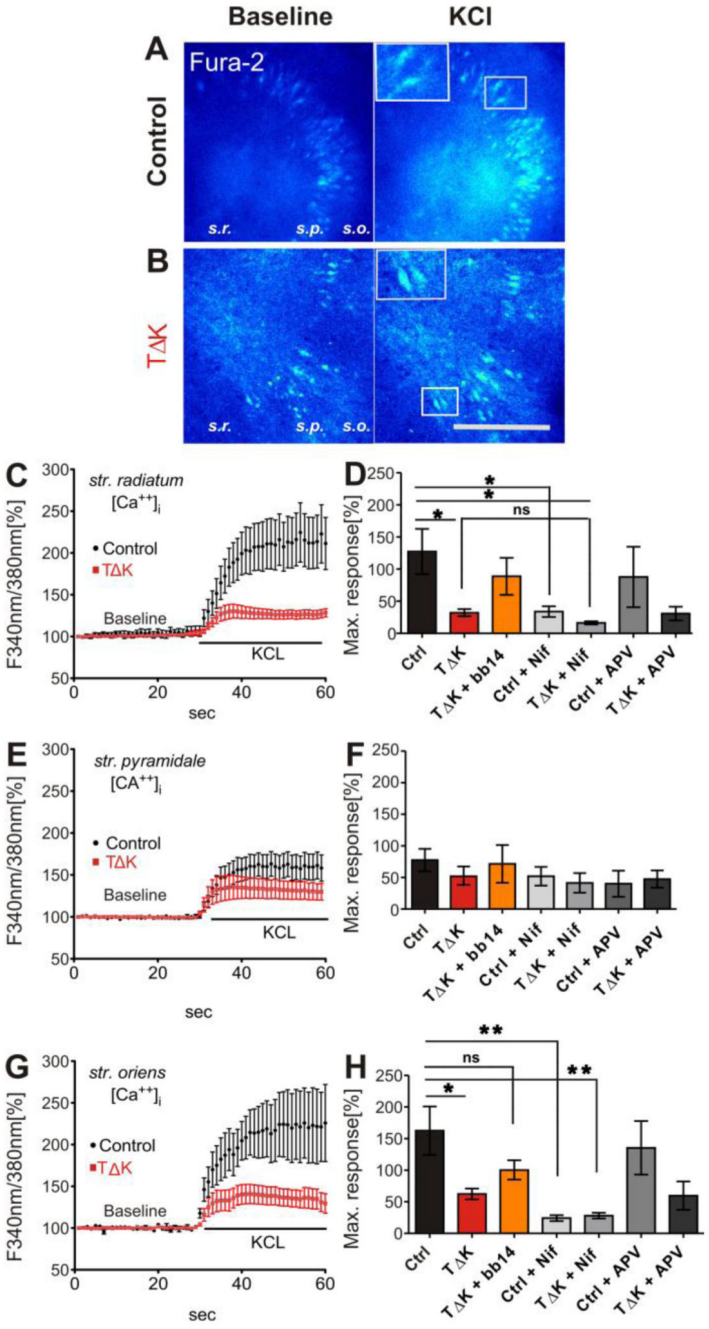

Fig. 5. Tau$_{RD}$ΔK attenuates Ca++ dynamics in area CA3.

(A, B) Slices (DIV15) from control (**A**) and Tau$_{RD}$ΔK mice (**B**) were loaded with the Ca++ indicator Fura-2AM. Ratio images (F340nm/380nm) are presented before membrane depolarization (baseline) and at the peak response to KCL application. Fura2-AM loading resulted in fluorescence of neurons as shown in the insets of A and B. The layers of area CA1-CA3, stratum radiatum (s.r.), stratum pyramidale (s.p.) and stratum oriens (s.o.) were analyzed consecutively.

(C, E, G) show the mean time course of $[Ca^{++}]i$ changes in response to high KCl. After depolarization $[Ca^{++}]i$ rises up to 250% of the initial levels in control slices (n=7, 4 different animals) in apical (s.r.) and basal (s.o.) dendrites. Cell somata in s.p. showed lower Ca++ responses (170%; n=7, 4 different animals). In contrast, in $Tau_{RD}\Delta K$ slices the Ca++ response was strongly attenuated in peak responses of all three layers (only 130%; averaged value; n=7, 4 different animals).

(D, F, H) Quantification of the maximum peak increase in intracellular Ca++ concentrations after high KCL stimulation. The strongest increase in $[Ca^{++}]i$ was observed in s.r. (ctrl 227%) and s.o.(ctrl 262%) whereas in s.p. the Ca++ response was only 177%. In $Tau_{RD}\Delta K$ slices the maximum response was strongly attenuated in str. radiatum ($F_{(6/29)}=3.796$; $p<0.05$) and str. oriens ($F_{(6/25)}=5.056$; $p<0.05$). This effect was partly rescued in the presence of bb14. The inhibition of L-VGCC by nifedipine (Nif, 20μM) inhibited the Ca++ influx of control slices to similar values as in $Tau_{RD}\Delta K$ slices without nifedepine apllication. The effect of nifedipine in $Tau_{RD}\Delta K$ slices was less prominent (n=5) compared with control slices. The application of the NMDAR blocker APV (100μM) reduced Ca++ influx only slightly in both control and in $Tau_{RD}\Delta K$ (n=3 and n=4 respectively). *One-way ANOVA* followed by Tukey's post-hoc test: ** p- value < 0.05, ** p-value < 0.01*. Scale bar in **A/B**: 200μM

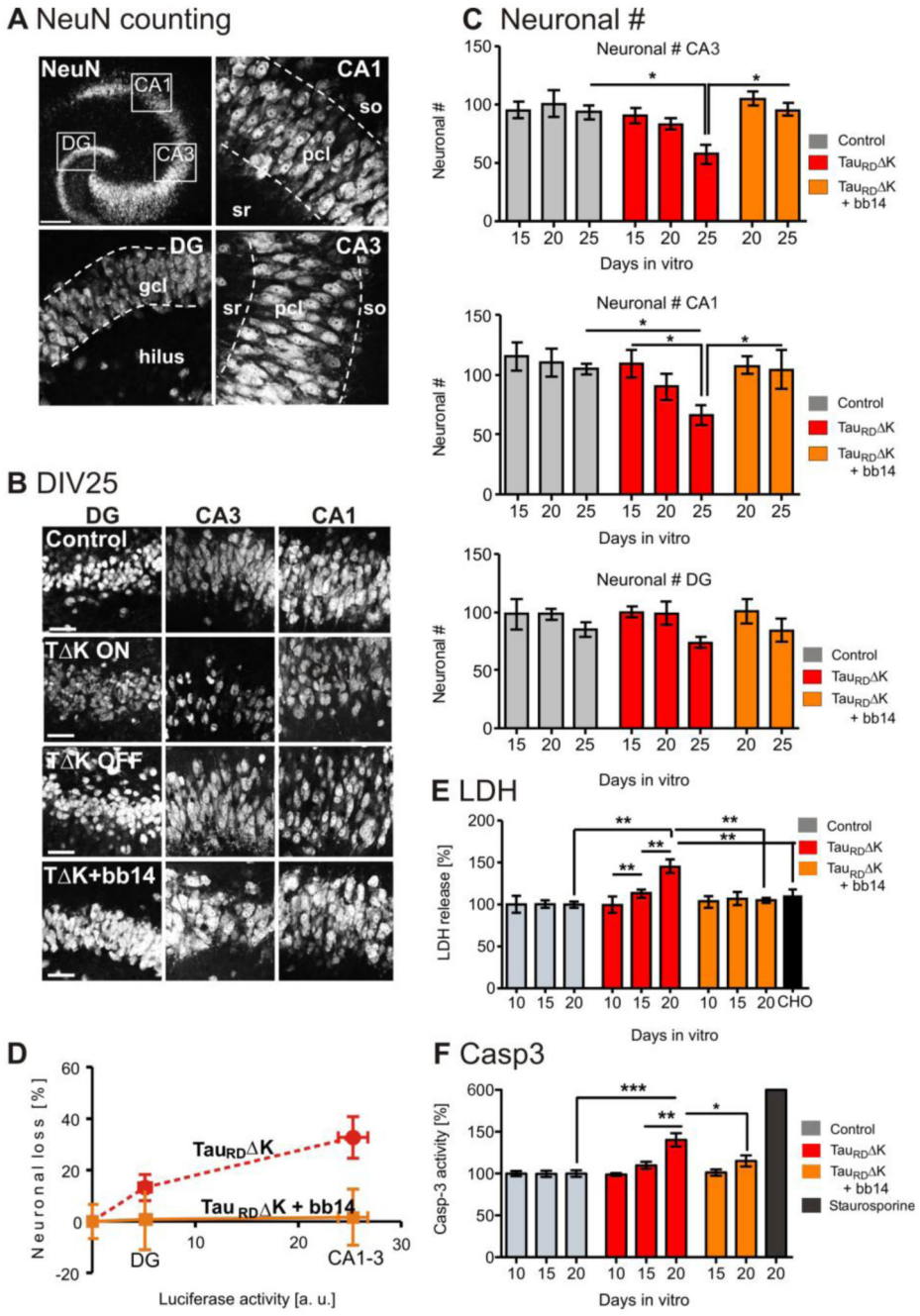

Fig. 6. Expression of $Tau_{RD}\Delta K$ causes neuronal loss via activation of caspase 3.

(A) NeuN positive cell bodies were counted in the DG and within the pyramidal cell layer in area CA1 and CA3 (dashed lines, slice at DIV25).

(B) Representative neuronal cell layers from slice cultures at DIV25: control, $Tau_{RD}\Delta K$ slices in switched-ON mode $Tau_{RD}\Delta K$ slices in switched-off mode (DOX treated for DIV1-DIV25) and $Tau_{RD}\Delta K$ slices in switched-on mode in the presence of compound bb14 (treated for DIV1-DIV25).

(C) Neurons in area CA1, CA3 and DG were counted at DIV15, 20 and 25 (8-10 slices, 6 animals/group). The number of neurons was strongly reduced in $Tau_{RD}\Delta K$ slices, both within area CA1 (-28%; $F_{(2/30)}$=4.405; p<0.05) and CA3 (-37%; $F_{(2/31)}$= 5.410; p <0.05) at DIV25 in comparison to control slices. This effect was already observed at DIV20 (CA1 (-18%) and CA3 (-16%) (not significant) and less prominently at DIV15 (CA1 (-6%) and CA3 (-5%). The neuronal number of the DG was only slightly reduced at DIV25 (-14%) and unaffected at earlier time points. Neuronal loss could be prevented by compound bb14 (15μM, starting at DIV1) in all the subregions (e.g. CA3 (only 3% (DIV20) and 7% (DIV25)).

(D) Correlation between $Tau_{RD}\Delta K$ expression (determined by reporter gene activity) and neuronal loss. The high expression of $Tau_{RD}\Delta K$ in the pyramidal cell layer causes a strong neuronal loss, but not in the DG where the expression level was much lower (Pearson r = 0.9759, linear regression test).

(**E**) LDH release (cytotoxicity) was analyzed in $Tau_{RD}\Delta K$, $Tau_{RD}\Delta K$+bb14, $Tau_{RD}\Delta K$ +DEVD-CHO and control slices at 10, 15 and 20 DIV. A pronounced increase (~40%; $F_{(3/19)}$=7.736; p<0.001) in LDH release was observed due to $Tau_{RD}\Delta K$ expression at 20 DIV but not at 10 DIV. At DIV15 the LDH release was slightly increased by 13% in $Tau_{RD}\Delta K$ expressing slices. The presence of bb14 rescued the effect on LDH release at 20 DIV to control levels. Treatment of slice cultures with the caspase-3 inhibitor DEVD-CHO strongly prevents LDH release when comparing $Tau_{RD}\Delta K$, TauRDΔK+bb14, $Tau_{RD}\Delta K$+DEVD-CHO and control slices.

(F) Caspase 3 activity was analyzed in $Tau_{RD}\Delta K$, $Tau_{RD}\Delta K$+bb14 and control slices at DIV 10, 15 and 20. Caspase 3 activity was unchanged at DIV10. $Tau_{RD}\Delta K$ expression caused an increase in caspase 3 activity by 10% (DIV15) and a significant increase by 35% ($F_{(2/16)}$=12.20; p<0.001) (DIV20), compared with slices from control mice. Treatment with bb14 relieved apoptosis (p<0.05). Apoptosis inducer staurosporine (0.5 μM for 24 hours) increased the caspase 3 activity by ~600%.

One-way ANOVA followed by Tukey's post-hoc test: *p < 0.05; **p < 0.01 and ***p < 0.001. Scale bars: **A,** upper panel, 200μm; **A**, lower panel, **B,** 50μM.

Europe PMC Funders Author Manuscripts

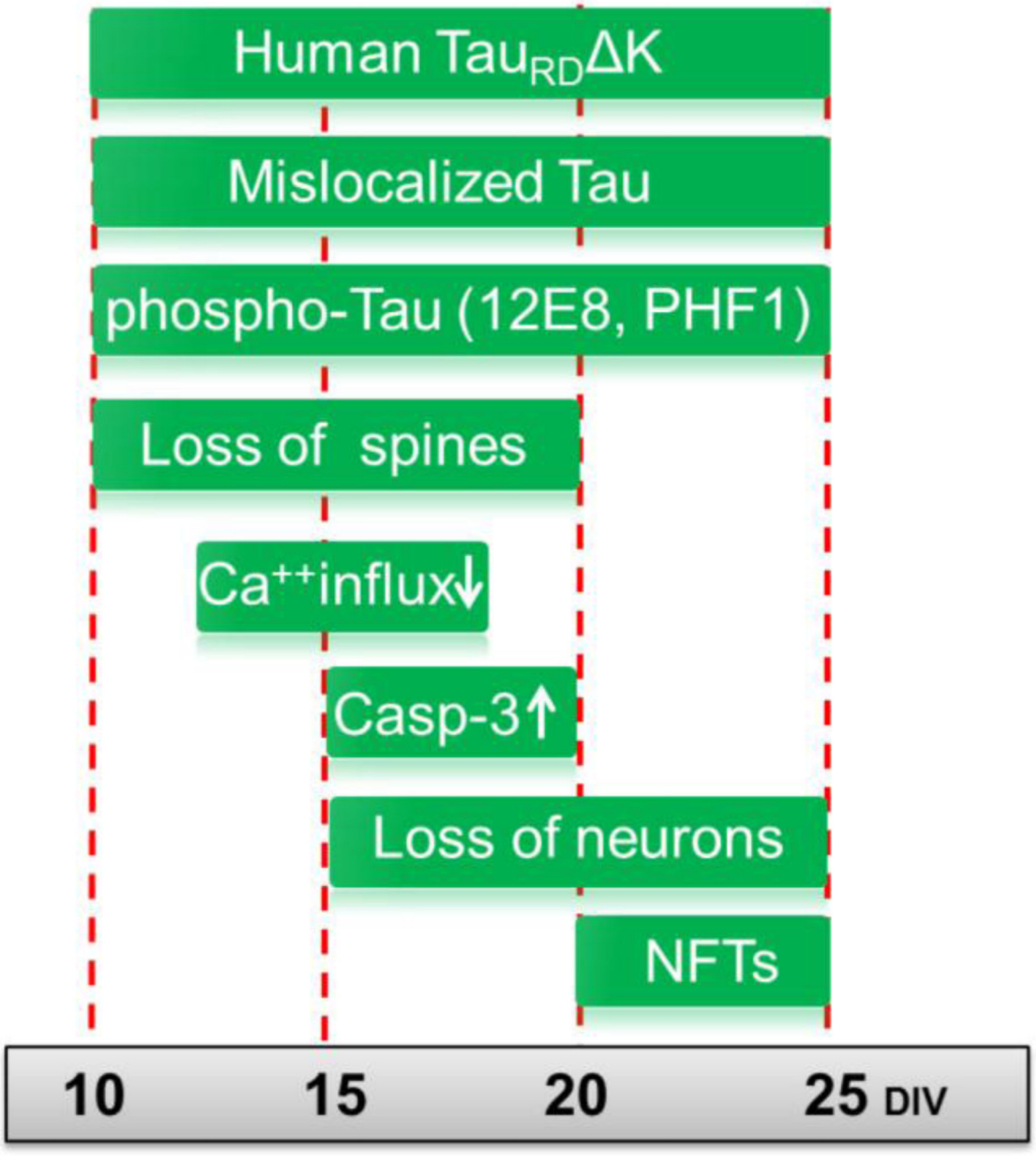

Fig. 7. Summary of pathological changes in pro-aggregant Tau$_{RD}$ΔK slices.

Tau$_{RD}$ΔK expressing mice were used for slice preparation at postnatal day 8. Cultures were analyzed up to 25 days in vitro (DIV). Early pathological events include the mislocalization of both endogenous and exogenous Tau into the somatodendritic compartment, observed already at DIV5 and remaining apparent until DIV25. From DIV10 onwards Tau becomes detectable in dendritic spines, and phospho-Tau appears in apical dendrites indicating mislocalization of endogenous Tau. At the same time (DIV10) the number of dendritic spines becomes strongly reduced. This is still observed at a later time point (DIV20), when

spines in $Tau_{RD}\Delta K$ slices are in an immature state. This effect is also observed in apical dendrites of pyramidal neurons and correlates with impairment in Ca++ dynamics, especially in stratum radiatum at DIV15. ThS positive Tau aggregates (neurofibrillary tangles (NFTs)), consisting of human and mouse Tau, are first detected at DIV20 and more prominently at DIV25. An increase in neuronal cell death (measured by LDH release, loss of NeuN) is first observed at DIV15 and increases further at DIV20 and DIV25. The activity of the apoptosis marker caspase 3 increases in parallel.

Europe PMC Funders Author Manuscripts